Inorganic Chemistry

pubs.acs.org/IC

Article

Contrasting Structure and Bonding of a Copper-Rich and a Zinc-Rich Intermetalloid Cu/Zn Cluster

Max Schütz, Maximilian Muhr, Kerstin Freitag, Christian Gemel, Samia Kahlal, Jean-Yves Saillard, Augusto C. H. Da Silva, Juarez L. F. Da Silva, Thomas F. Fässler, and Roland A. Fischer*

Cite This: https://dx.doi.org/10.1021/acs.inorgchem.0c00943

Read Online

ACCESS | Metrics & More | Article Recommendations | Supporting Information

ABSTRACT: Reaction of the Cu(I) sources, $[Cu_5](Mes)_5$ and $[(^{i}Dipp)CuO^{t}Bu]$ (Mes = mesityl; ^{i}Dipp = 1,3-bis(2,6-diisopropylphenyl)-1*H*-imidazol-2-ylidene) with the Zn(I) complex $[Zn_2](Cp^*)_2$ leads to a mixture of intermetallic Cu/Zn clusters with a distribution of species that is dependent on the stoichiometric ratio of the reactants, the reaction time, as well as the temperature. Systematic and careful investigation of the product mixtures rendered the isolation of two new clusters possible, *i.e.*, the Zn-rich, red cluster **1**, $[CuZn_{10}](Cp^*)_7 = [Cu(ZnZnCp^*)_3(ZnCp^*)_4]$, as well as the Cu-rich, dark-green cluster **2** $[Cu_{10}Zn_2](Mes)_6(Cp^*)_2$. Structure and bonding of these two species was rationalized with the help of density functional theory calculations. Whereas **1** can be viewed as an 18-electron Cu center coordinated to four ZnCp* and three ZnZnCp* one-electron ligands (with some interligand bonding interaction), compound **2** is better to be described as a six-electron superatom cluster. This unusual electron count is associated with a prolate distortion from a spherical superatom structure. This unexpected situation is likely to be associated with the ZnCp* capping units that offer the possibility to strongly bind to the top and the bottom of the cluster in addition to the bridging mesityl ligands stabilizing the Cu core of the cluster.

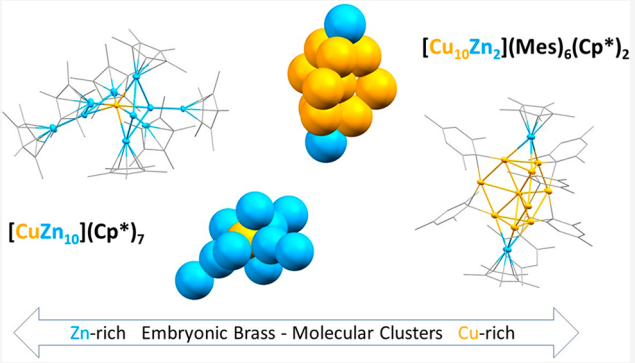

INTRODUCTION

We have been interested for a long time in the synthesis of bimetallic, molecular complexes and cluster compounds, accessible by bottom-up synthesis from low valent ECp* ligands (E = Al, Ga, In, Zn) and organometallic transition metal (TM) precursors.[1,2] Especially for late transition metals (TMs), many examples for intermetallic complexes $[TM_a(ECp^*)_b(L)_c]$ and clusters $[TM_aE_b](R_c)$ (R = hydrocarbon ligand such as Me = CH_3, Cp* = $C_5(CH_3)_5$, $CN^{t}Bu$, etc.) could be isolated and structurally characterized.[1,2] In particular, a variety of intermetallic Cu/Zn clusters are accessible, some of which show structural similarities to the solid-state structures of brass phases. The molecular structure of the superatom cluster $[Cu_4Zn_4](CN^{t}Bu)_4(Cp^*)_4$, for example, is based on interpenetrated Cu_4 and Zn_4 tetrahedra with a $[Cu_4Zn_4]$ unit (M_8), which is also found in γ-brass.[3] The triangular cluster $[CuZn_2](Cp^*)_3$ has been identified as an "embryonic" building block of such brass clusters.[4] The species $[CuZn_2](Cp^*)_3$ does indeed give access to larger clusters in defined cluster building up reactions: in the presence of the substitutionally labile Zn(I) dimer $[Zn_2]Cp^*(L)_3^+$ (L = Et_2O), the cationic M_7 cluster $\{[Cu_2Zn_5](Cp^*_5)\}^+$ is formed.[4,5] The isoelectronic neutral analogue $[Cu_3Zn_4](Cp^*)_5$ is obtained by reaction of Cu(OAc) with $[Zn_2](Cp^*)_2$ in very low yields.[5] Both M_7 clusters are isoelectronic and highly electron deficient according to Wade-Mingos rules; remarkably, Cu 3d orbitals contribute substantially to cluster bonding.[5] In all examples of molecular "embryonic brass" clusters reported so far, the Cu/Zn ratio is not far away from 1:1 with a slight bias to zinc, ranging from 1:1 in $[Cu_4Zn_4](CN^{t}Bu)_4(Cp^*)_4$ to 1:2.5 in $[Cu_2Zn_5](Cp^*)_5^+$.

The bimetallic metal cores of such M/E clusters are most often structurally similar to cut-outs of the respective intermetallic solid-state phases. "Structural similarity" includes the appearance of similar structural motifs such as polyhedral shapes or metal coordination numbers but also similar interatomic distances as in intermetallic compounds. While the electronic situation in extended solid-state phases is doubtlessly different from that in a finite molecular cluster, the underlying electronic principles may well be associated, *e.g.*, the polarization of M−M′ interactions triggered by the different

Received: March 30, 2020

Scheme 1. Synthesis of Cluster 1, $[CuZn_{10}](Cp^*)_7$ = $[Cu(ZnZnCp^*)_3(ZnCp^*)_4]$[a]

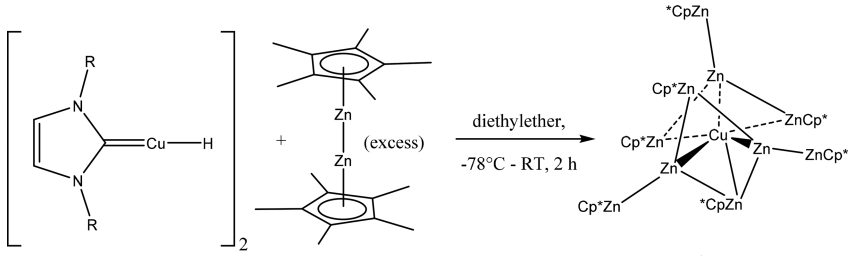

1

[a]R = 2,6-diisopropylphenyl. The Cu−Zn connecting lines illustrate short contacts.

electronegativities of the two metals. In the case of solid-state brass phases, the Cu/Zn ratio has a strong influence on the structural and physical properties of the materials. For example, below 2:1, α-brass exhibits a regular fcc structure based on that of metallic Cu. With increasing zinc content β-brass, a bcc structure is favored. Only with zinc contents above 50% are the structurally diverse Hume−Rothery phases γ-, δ-, and ε-brass are observed.[6] Even though it has been known for a long time that the structures of Hume−Rothery phases strongly correlate with the average valence-electron concentration (VEC) of the distinct compositions such as β-, γ-, and ε-brass with VEC = 1.5 (CuZn), 1.615 (Cu_5Zn_8), and 1.75 ($CuZn_3$), respectively, no simple chemical picture exists for their understanding.[7] Thus, the exploration of the structural variability of molecular Cu/Zn clusters is an interesting target to us. How are the electronic situations and bonding properties in such clusters affected if the abundance of one of the two metals is much higher than the other? In this contribution, we like to present the synthesis and characterization based on experimental techniques and density functional theory calculations of two new molecular Cu/Zn clusters with metal core compositions far away from Cu/Zn = 1:1. Specifically, we succeeded in the isolation and characterization of the Zn-rich cluster $[CuZn_{10}](Cp^*)_7$ (**1**) as well as its Cu-rich congener $[Cu_{10}Zn_2](Mes)_6(Cp^*)_2$ (**2**).

EXPERIMENTAL SECTION

General. All experiments were conducted using standard Schlenk and glovebox techniques under an atmosphere of purified argon. All solvents were carefully dried (water content < 5 ppm) and saturated with argon prior to their use. The starting compounds $[Zn_2](Cp^*)_2$, CuMes = $[Cu_5](Mes)_5$, and $[(^i\text{Dipp})\text{CuO}^t\text{Bu}]$ were prepared according to literature methods.[8−10] For both compounds **1** and **2**, no meaningful data for elemental analyses (C, H, Cu, Zn) could be obtained due to their high sensitivity (**2**) as well as cocrystallization with side products (**1**). However, in both cases, the molecular ion signal in the LIFDI (liquid field injection desorption ionization) mass spectrum is consistent with the suggested elemental composition derived from crystallographic and other spectroscopic data. NMR spectra were recorded on a Bruker Avance III AV400US (^{1}H, 400 MHz; ^{13}C 101 MHz) and a Bruker Avance II 500 with a cryoprobe (^{13}C, 125 MHz). Variable temperature (VT) NMR spectra were recorded on a Bruker DRX 400 spectrometer (^{1}H, 400 MHz). Chemical shifts are described in ppm relative to tetramethylsilane (TMS) and referenced to the solvent residual signals. Mass spectrometry was conducted with a Micromass LCT-Q-TOF micro mass spectrometer and a Thermo-Fischer Exactive Plus mass spectrometer using LIFDI as ionization method. Raman scattering was performed on a Renishaw inVia Raman microscope RE04 using an excitation wavelength of 532 nm. The data were collected with a CCD detector and evaluated using WiRE 4.2. FT-IR spectra were measured in an ATR setup with a Bruker Alpha FTIR spectrometer under an inert gas atmosphere in a glovebox. Data for X-ray crystallography were collected on a single crystal X-ray diffractometer equipped with a TXS rotating anode and an IMS microsource (see Table S1) with Mo K_α radiation (λ = 0.71073 Å) and a Helios optic using the APEX3 software package. Measurements were performed on single crystals coated with perfluorinated ether. The crystals were fixed on top of a Kapton micro sampler and frozen under a stream of cold nitrogen. Diffraction data were processed using the APEX3 software with the implemented SAINT and SADABS programs. The structures were solved using SHELXT with the aid of successive difference Fourier maps and were refined against all data using SHELXL-2014/2017 in conjunction with SHELXLE. The unit cell of compound **1** contains one disordered molecule of diethyl ether, which was treated as a diffuse contribution to the overall scattering without specific atom positions using the PLATON/SQUEEZE procedure. The unit cell of compound **2** contains six disordered molecules of toluene, which were treated as a diffuse contribution to the overall scattering without specific atom positions using the PLATON/SQUEEZE procedure. We refer to the Supporting Information for a more detailed procedure for X-ray crystallography and refinement including literature references for the used programs and software.

Synthesis of $[CuZn_{10}](Cp^*)_7$ = $[Cu(ZnZnCp^*)_3(ZnCp^*)_4]$ (1). A sample of 274 mg (0.52 mmol) of $[(^i\text{Dipp})\text{Cu}(O^t\text{Bu})]$ was suspended in 8 mL of diethyl ether and cooled to −75 °C. A volume of 0.15 mL of $[HSi(OEt)_3]$ (0.81 mmol) was added dropwise to the solution leading to an immediate color change to yellow. The solution was stirred for 4 h at −75 °C before a solution of 420 mg of $[Zn_2](Cp^*)_2$ (1.0 mmol) in 7 mL of diethyl ether was added at that temperature. The resulting solution was allowed to warm to room temperature and stirred for 2 h, accompanied by a color change to deep-red. The solution was concentrated in vacuum, filtered, and left for crystallization at −30 °C for several weeks leading to a mixture of red crystals of **1** and colorless ones of $[Zn_2](Cp^*)_2$, which was isolated and washed with a minimum amount of *n*-hexane. The yield could not be determined due to the inseparability of the two types of crystals. The assignment of the spectroscopic data of the manually separated single crystals of **1** is as follows: ^{1}H NMR (298 K, 400 MHz, C_6D_6, manual separation of single crystals): 2.22 (s, 105H, Cp*). ^{1}H NMR (208 K, 400 MHz, C_6D_6, manual separation of single crystals): 2.25 (s, 45H, ZnZnCp*), 2.27 (s, 60H, ZnCp*). ^{13}C NMR (298 K, 400 MHz, C_6D_6, manual separation of single crystals): 12.21 (s, $C_5(\underline{C}H_3)_5$ groups), 111.10 (s, $\underline{C}_5(CH_3)_5$). Raman (298 K): ν [cm^{-1}] = 2850 (b, w), 1575 (b), 1025 (s, w), 980 (s), 142 (s); (see Supporting Information, Figure S5). LIFDI-MS: *m*/*z* (a.u.) = 1664 ($[M]^+$), 1462 ($[M\text{-}ZnCp^*]^+$).

Synthesis of $[Cu_{10}Zn_2](Mes)_6(Cp^*)_2$ (2). A sample of 200 mg (1.1 mmol) of [CuMes] = $[Cu_5](Mes)_5$ and 132 mg (0.3 mmol) of $[Zn_2](Cp^*)_2$ were dissolved in 25 mL of toluene and heated to 75 °C for 7 days. The dark solution was filtered via a passivated glass frit, concentrated under reduced pressure (4 mL), and left for crystallization at −30 °C for several weeks. Dark-green crystals of **2** were isolated in 9.1% yield (based on Cu) and washed with a minimum amount of *n*-hexane (3 × 0.3 mL). ^{1}H NMR (298 K, 400 MHz, C_6D_6): 1.62 (s, 30 H, ZnCp*), 2.03 (s, 18H, CH_3 (Mes)), 2.67 (s, 36H, CH_3 (Mes)), 6.76 (s, 12H, CH_{aryl}(Mes)). ^{13}C NMR (298 K,

https://dx.doi.org/10.1021/acs.inorgchem.0c00943
Inorg. Chem. XXXX, XXX, XXX−XXX

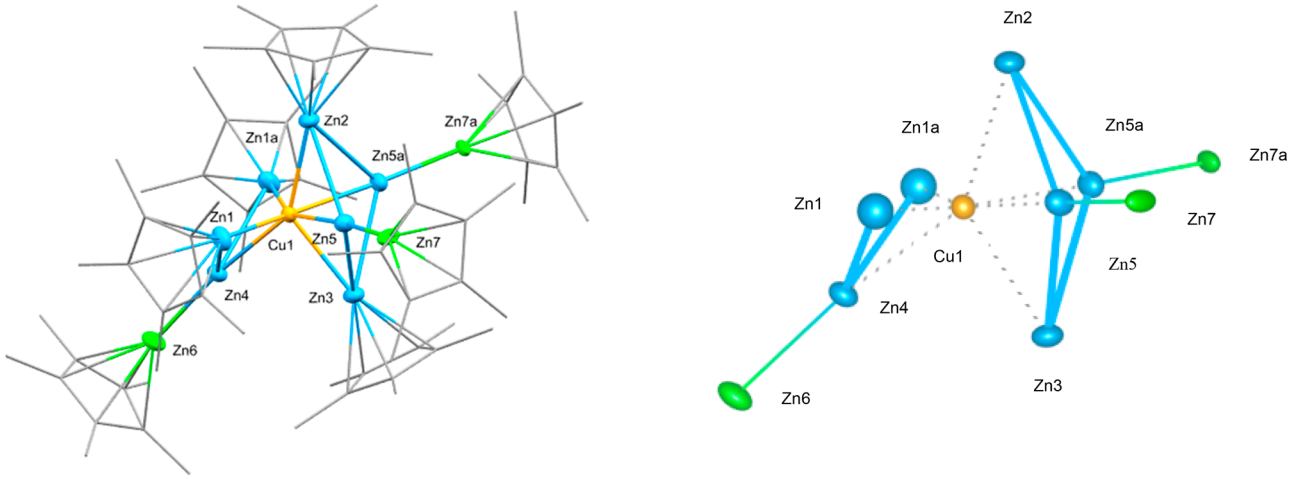

Figure 1. Left: Molecular structure of **1** in the solid state as determined by SC-XRD. Thermal ellipsoids are shown at the 50% probability level; hydrogen atoms, cocrystallized solvent molecules, and disordered groups are not shown for clarity, and ligands are simplified as wireframes. Selected interatomic bond distances [Å] and angles [°]: Cu1−Zn5: 2.3477(3), Cu1−Zn1: 2.335(5), Cu1−Zn2: 2.3997(5), Cu1−Zn4: 2.3662(4), Cu1−Zn3: 2.4136(5), Zn4−Zn6: 2.3686(5), Zn5−Zn7: 2.390(5), Zn2−Zn5: 2.7489(4), Zn1−Zn4: 2.713(6), Zn5−Zn3: 2.7418(4), Cu1−Zn4−Zn6: 173.08(2), Cu1−Zn5−Zn7: 172.0(2). Right: Coordination geometry of Cu (orange) in **1** with Zn in the first (blue) and second coordination sphere (green). Longer Zn−Zn contacts are illustrated in blue, and shorter ones are illustrated as a blue-green gradient line.

400 MHz, C_6D_6): 9.41 (s, methyl groups (ZnCp*)), 21.18 (s, methyl groups (Mes)), 30.49 (s, methyl groups (Mes)), 110.23 (s, ring carbon atoms (Cp*)), 126.52 (s, ring carbon atoms (Mes)), 137.46 (s, ring carbon atom (ZnCp*)), 140.57 (s, ring carbon atoms (Mes)), 154.68 (s, ring carbon atoms (Mes)). ATR-IR (298 K): ν [cm^{-1}] = 3011 (w), 2962, 2908, 2855, 1594 (s), 1444, 1413, 1380, 1283 (w), 1258 (s, (i), 1081 (i), 1013 (i), 863 (w), 842 (w), 791 (i), 661−698, 574 (w), 544 (w), 527 (w); (see Supporting Information, Figure S8). LIFDI-MS: m/z (a.u.) = 1751 ($[M]^+$).

RESULTS AND DISCUSSION

Synthesis and Characterization of the Zinc-Rich M_{11} Cluster $[CuZn_{10}](Cp^*)_7$ (1). *Synthesis.* The reaction conditions for the synthesis of **1** are described in Scheme 1. The reaction progress can be monitored by LIFDI-MS pointing to the formation of various Cu(^{i}Dipp) aggregates as well as of a complicated mixture of $M_8/M_{11}/M_{13}$ mixed metal Cu/Zn clusters (see figure S1). However, when the concentrated reaction solution is cooled down to −30 °C, single crystals of $[CuZn_{10}](Cp^*)_7$ (**1**) are formed as deep-red octahedral fragments as well as colorless crystals of unconsumed $[Zn_2](Cp^*)_2$. Cluster **1** can only be manually separated from $[Zn_2](Cp^*)_2$ by crystal picking under an optical microscope in the glovebox; however, an analytically quantitative separation of the crystals is not possible. All attempts to purify compound **1** by washing or recrystallization from different solvents failed due to the very similar solubilities of **1** and $[Zn_2](Cp^*)_2$, and therefore, unfortunately, no meaningful data for elemental analysis were obtained.

Cluster **1** readily dissolves in common organic solvents (toluene, benzene, hexane, diethyl ether), and solutions in benzene are stable at room temperature for several days before slow decomposition (metallic precipitate) occurs.

Notably, the excess of $[Zn_2](Cp^*)_2$ in the synthesis of **1** is crucial. The use of stoichiometric amounts leads to unspecific reaction mixtures, and no product can be isolated. Obviously, high concentrations of $[Zn_2](Cp^*)_2$ are required to "trap" the Cu fragments formed in the competitive thermal decomposition of ^{i}Dipp−Cu−H. Due to the chemical instability of ^{i}Dipp−Cu−H, we also investigated the reaction of the thermally more stable analogous PPh_3 compound $[Cu_6](H)_6(PPh_3)_6$. However, Cp* transfer to copper was observed in this case as the dominating mechanism, and the thermodynamically very stable half-sandwich complex $[(PPh_3)CuCp^*]$ was isolated as the only product. This illustrates the importance of the choice of the organometallic Cu source and thus points to the kinetic control of the Cu/Zn cluster formation reactions.

Crystallographic Characterization of 1. The molecular structure of **1** in the solid state has been investigated by SC-XRD (see Figure 1). We refer to the Supporting Information (Table S1) for detailed crystallographic information. Cluster **1** crystallizes in the orthorhombic space group *Pnma* with four molecules per unit cell together with four molecules of heavily disordered diethyl ether per asymmetric unit. The molecule of **1** sits on a crystallographic symmetry plane and thus possesses C_s symmetry. The central Cu atom is heptacoordinated by three Zn−ZnCp* units and four ZnCp* units. In all seven Zn units, the protecting Cp* ligands are η^5-coordinated, with Zn−$Cp^*_{centroid}$ distances varying between 1.91 and 2.01 Å, which is typical for Zn−Cp* distances found in the literature (*e.g.* 1.934 Å for $[Pd(ZnCp^*)_4(ZnMe)_4]$).[11] The distances of the central Cu to the surrounding Zn atoms lie between 2.335(5) and 2.3997(5) Å, which is comparable to that found in the triangular cluster $[CuZn_2](Cp^*)_3$ (2.381(1) Å) and indicates a dense sphere packing structure motive for **1**.[4] Notably, the Cu−ZnCp* distances (2.3997(5) for Cu1−Zn2 and 2.4136(5) for Cu1−Zn3) are distinctly longer than the Cu−ZnZnCp* distances (2.3477(3)and 2.3477(4) Å) with exception of the Cu1−Zn1 bond (2.335(5) Å). This phenomenon has also been observed in $[Pd(ZnCp^*)_4(ZnZnCp^*)_4]$.[12] The Zn−Zn bond lengths within the Zn_2 units in **1** are 2.3686(5) Å (Zn4−Zn6) and 2.390(5) Å (Zn5−Zn7), *i.e.*, they are elongated by 3−4% with respect to $[Zn_2](Cp)^*_2$ (2.305 Å).[8] They are also significantly longer than those reported for $[Cu_3Zn_4](Cp^*)_5$ and $\{[Cu_2Zn_5](Cp^*_5)\}^+$ (2.299(6) − 2.318(2) Å).[5] The Zn−Zn−Cu moieties further show a significant deviation from linearity (Cu1−Zn4−Zn6: 173.08(2)° and Cu1−Zn5−Zn7: 172.0(2)°). Longer Zn···Zn contacts (2.713(6)−2.7489(4)Å)

https://dx.doi.org/10.1021/acs.inorgchem.0c00943
Inorg. Chem. XXXX, XXX, XXX−XXX

are also present between the Zn atoms coordinated to Cu. This is a characteristic feature of late transition-metal complexes of ZnR (R = Cp*, ZnCp*, Me).[13] Considering these contacts, the whole coordination sphere around Cu can be viewed as made up of two parts, a bent [(Cp*Zn)(ZnZnCp*)(ZnCp*)] assembly (Zn1−Zn4−Zn1a in Figure 1) as well as a [(Cp*Zn)(ZnZnCp*)(ZnCp*)(ZnZnCp*)] folded diamond (Zn2−Zn5−Zn3−Zn5a in Figure 1). The symmetry plane cuts each of these two pieces in two equivalent halves, with Zn(2), Zn(3), and Zn(4) lying on it as well as Cu (see figure. 1).

Spectroscopic Characterization of **1**. The ^{1}H NMR spectrum at room-temperature (Figure S2) of isolated single crystals of **1** in benzene-d_6 reveals one sharp singlet at 2.22 ppm beside a small signal attributable to $[Zn_2](Cp^*)_2$ at 2.03 ppm. The occurrence of only one signal for all the Cp* ligands of **1** is surprising, as the symmetry of the molecule in the solid state suggests five distinct signals in the Cp* region, *i.e.*, two singlets for the Zn−ZnCp* ligands with an integral ratio of 2:1 as well as three signals for ZnCp* ligands with an integral ratio of 2:1:1. At −90 °C in toluene-d_8, a splitting of the room temperature signal at 2.22 ppm into two discrete singlets at 2.23 and 2.25 ppm with an integral ratio of 3:4 is observed (see Figure S2, bottom). Obviously, a fast exchange of all Cp* ligands is observed at room temperature, involving exchange between ZnCp* and ZnZnCp* ligands. Whether this exchange process is based on Zn−Zn or Zn−Cp* bond cleavage is not clear and cannot be decided on VT-NMR data only. The ^{13}C NMR spectrum of **1** in benzene-d_6 at room temperature shows two signals at 12.21 and 111.10 ppm (Figure S3). Unfortunately, no ^{13}C NMR spectrum could be recorded at −90 °C, due to decreased solubility of the compound at low temperatures.

The molecular ion peak of $[CuZn_{10}](Cp^*)_7$ is detected as a weak signal at m/z = 1664 (see Figure S4). Unfortunately, the isotopic pattern observed for the molecular ion peak does not satisfy high resolution standards (see Figure S4, right) due to the weak intensity of the signal. However, the fragment ion $[\mathbf{1} - ZnCp^*]^+$ is observed with high resolution, and its isotopic pattern is well consistent with the calculated one for $[CuZn_9](Cp^*)_6$ (see Figure S4, left).

Computational Analysis of **1**. The assignment of the copper location in **1** was obtained by geometry optimizations based on total energy DFT calculations of seven representative configurations (see Supporting Information, Figure S10) corresponding to different occupations of the metal positions, using the all-electron full-potential Fritz−Haber institute *ab initio* molecular simulations (FHI-aims) package[14] with the PBE functional[15] (see computational details, Supporting Information). Unsurprisingly, the most stable structure is that with copper lying at the central position (see Supporting Information, figure S10), in full agreement with the above-discussed spectroscopic and structural data. It lies 0.67 eV below in energy than the next most stable configuration, in which Cu is located at a more peripheral position. In a following step, using the lowest energy structure, the electronic structure of **1** was then analyzed by using the ADF program suite[16,17] at the BP86/TZ2P-D3 level (see computational details, Supporting Information). Although slightly distorted away from C_s symmetry, the optimized geometry of **1** at this level of theory was found to be close to its X-ray structure. The computed ^{1}H NMR chemical shifts (av. 2.06 and 1.95 ppm for ZnCp* and ZnZnCp*, respectively) as well as the ^{13}C chemical shifts (av. 10.66 and 113.16 ppm for ZnCp* and av. 7.74 and 111.57 ppm for ZnZnCp*) are consistent with the experimental data. Discarding first the long Zn···Zn contact and considering that each individual ZnCp* or ZnZnCp* unit is a 1-electron donor, the 7 electrons provided by the seven organozinc ligands add up to the 11 valence electrons of Cu(0), making later an 18-electron metal center. This electron count is consistent with the computed substantial HOMO−LUMO gap (2.06 eV). However, the 18-electron rule should be considered carefully when applied to complexes in which the number of ligands is larger than the number of metal valence orbitals available for bonding. In such situations, delocalization over the ligand sphere is expected. This is what happens in **1** where the $3d^{10}4s^1$ copper center has only four accepting orbitals (4s and 4p) to accommodate the seven ligand electrons coming from seven organozinc σ-type orbital combinations. These seven combinations interact with the Cu orbitals in a manner roughly sketched in Figure 2. Four among

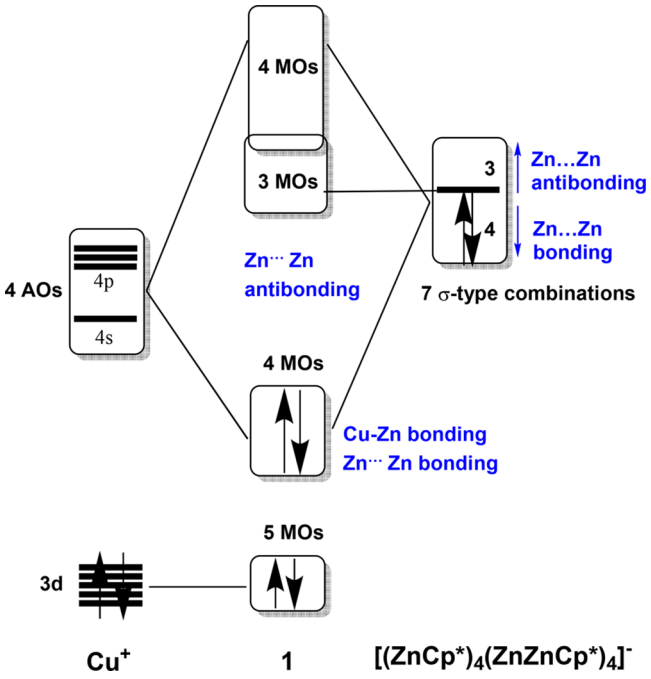

Figure 2. Simplified MO diagram sketching the interaction of the Cu valence AOs with the combinations of the σ-type frontier orbitals of the ZnCp* and ZnZnCp* fragments in **1**. For the sake of simplicity, Cu is considered in its +I oxidation state, making the whole ligand sphere an eight-electron donor system.

the seven organozinc combinations interact with the copper 4s and 4p orbitals, leaving three of them nonbonding with Cu. Among the seven organozinc combinations, those which are the closest in energy to the copper AOs are expected to interact in a stronger way. These orbitals are the lowest among the seven and thus are those which have Zn···Zn bonding character. In fact, they are the two lowest σ-type combinations (somewhat stabilized by 4p(Zn) AOs of the ZnZnCp* ligands) of each of the two subunits [(Cp*Zn)(ZnZnCp*)-(ZnCp*)] and [(Cp*Zn)(ZnZnCp*)(ZnCp*)(ZnZnCp*)]. On the other hand those having Zn···Zn antibonding character are expected to interact to a lesser extent. This is exemplified by a fragment decomposition analysis, which indicates that the four lowest σ-type organozinc combinations have a global occupation of 5.98 electrons, whereas that of three highest ones is only 1.03 electrons. It results that the highest occupied

https://dx.doi.org/10.1021/acs.inorgchem.0c00943
Inorg. Chem. XXXX, XXX, XXX−XXX

Scheme 2. Synthesis of Cluster 2, $[Cu_{10}Zn_2](Mes)_6(Cp^*)_2$

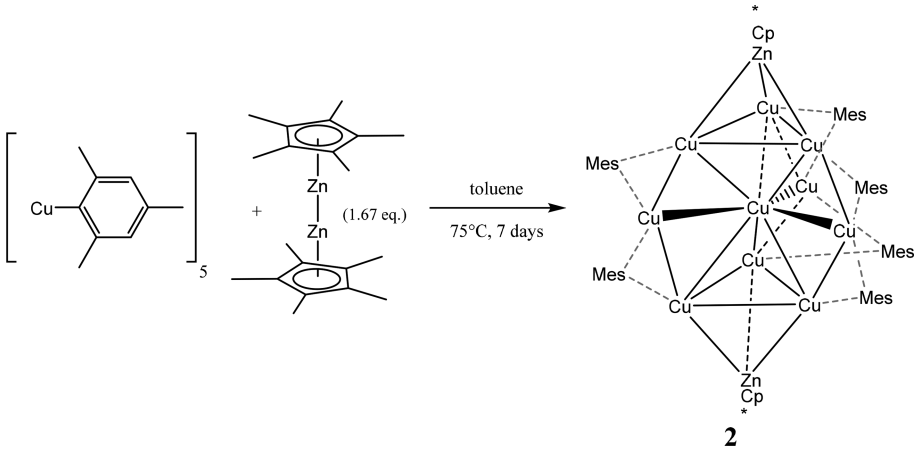

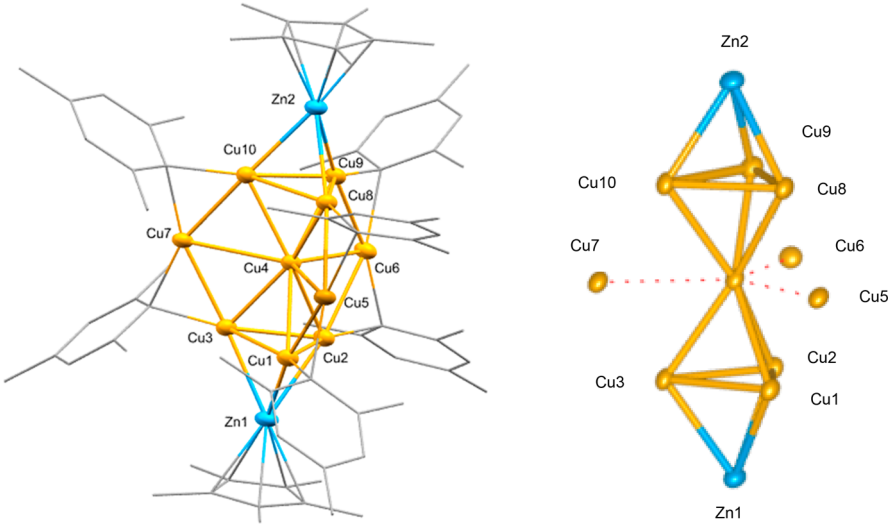

Figure 3. Left: Molecular structure of **2** in the solid state as determined by SC-XRD. Thermal ellipsoids are shown at the 50% probability level; hydrogen atoms, cocrystallized solvent molecules, and disordered groups are not shown for clarity, and ligands are simplified as wireframes. Selected interatomic bond distances [Å] and angles [°]: Cu4−Cu10: 2.4617(8), Cu1−Cu5: 2.4223(7), Cu4−Cu3: 2.4566(7), Cu4−Cu7: 2.7662(8), Cu10−Zn2: 2.4659(8), Cu3−Zn1: 2.4528(8), Cu10−Zn2: 2.4658(7), Cu3−Zn1: 2.4526(7), Cu7−$C_{bridging\ mesityl}$: 2.030(4), Cu3−$C_{bridging\ mesityl}$: 2.012(4), Zn1−$Cp^*_{centroid}$: 1.91, Zn2−$Cp^*_{centroid}$: 1.92, Cu7−$C_{bridging\ mesityl}$−Cu3: 52.54(13), Cu10−Cu4−Cu8: 59.85(2), Cu7−Cu4−Cu6: 118.60(2); Cu10−Zn2−Cu8: 59.30(2). Right: Cluster core geometry of **2** (Cu = orange, Zn = blue). Cu−Cu bonds are illustrated in orange, and Cu−Zn bonds are illustrated in orange-blue.

levels of **1** have some Zn···Zn bonding character, whereas those having Zn···Zn antibonding character are vacant. The diagram of Figure 2 is obviously oversimplified, but it allows explaining where bonding delocalization between the organozinc ligands originates from. It is worth noting that this situation is allowed, because the organozinc σ-type orbitals lie at higher energy than the 3d(Cu) block. A lower energy would result in the occupation of their Zn···Zn antibonding combinations. Steric crowding among the ligand sphere tends also to favor such delocalization. The availability of seven organozinc combinations to stabilize four Cu AOs is also favorable to a fluxional behavior of the organozinc ligand sphere around the copper center.

The four highest occupied orbitals in Figure 2 have substantial Cu character; the computed natural atomic orbital (NAO) charge of Cu is negative (−0.66). Consistently, the seven zinc atoms bonded to Cu have positive NAO charges (avg. +0.70), with the three outer zinc atoms being less polarized (avg. +0.48). The computed Cu−Zn Wiberg indices are consistent with Cu−ZnCp* covalent bonding significantly stronger than Cu−ZnZnCp* bonding (avg. 0.255 and 0.094, respectively). Unsurprisingly, the computed Zn···Zn Wiberg indices (avg. 0.084) are much smaller than that corresponding to the Zn−Zn single bonds (avg. 0.490).

Synthesis and Characterization of the Copper-Rich M_{12} Cluster $[Cu_{10}Zn_2(Mes)_6Cp^*_2]$ (2). *Synthesis of* **2**. The synthesis of $[Cu_{10}Zn_2](Mes)_6(Cp^*)_2$ (**2**) is described in Scheme 2. Compound **2** was identified as the major reaction product by LIFDI-MS (see Figure S9). After cooling the filtered and concentrated reaction solution to −30 °C, **2** can be separated from the mixture in form of very air- and moisture-sensitive black-green crystals (see Scheme 2). The molecular structure of **2** in the solid state has been determined by SC-XRD (see Figure 3).

Cluster **2** is well soluble in toluene but less soluble in benzene and only sparingly soluble in hexane. It can be obtained in analytically pure form after the isolated crystals are washed with hexane. It is only moderately stable under argon

https://dx.doi.org/10.1021/acs.inorgchem.0c00943
Inorg. Chem. XXXX, XXX, XXX−XXX

atmosphere at room temperature in the solid state as well as in solution. Prolonged heating to more than 100 °C leads to the formation of a metallic precipitate. Due to the high sensitivity of **2**, no meaningful data from elemental analysis could be obtained.

Crystallographic Characterization of ***2***. Cluster **2** crystallizes in the triclinic space group *P*-1 with two molecules per unit cell and three disordered molecules of toluene per asymmetric unit. We refer to the Supporting Information (Table S1) for detailed crystallographic information. The metal core structure of **2** is close to ideal D_{3h} symmetry and consists of two vertex-sharing tetrahedra Cu1−Cu2−Cu3−Cu4 and Cu4−Cu8−Cu9−Cu10 with Cu4 as the central vertex of both tetrahedra. The edges of this Cu_7 unit are bridged by three more Cu atoms (Cu5, Cu6, Cu7) forming a Cu_3 triangle around the central Cu4. Both tetrahedra are additionally capped by Zn atoms with an almost linear arrangement of Zn1−Cu4−Zn2. Most interestingly, the structural motif of two edge-sharing Cu_4 tetrahedra is also found in LAVES phases such $MgCu_2$.[18]

The Cu−Cu distances within the cluster core are all between 2.4223(7) and 2.7662(8) Å, which is well within the range of molecular compounds with direct Cu−Cu bonds reported in literature (2.3 Å for $\{^{i}DiPPCuH\}_2$,[19] 3.424 Å for $\{[Ag_6Cu_2(dppe)_3(CCC_6H_4OCH_3)_6(MeCN)](ClO_4)_2\}$ (dppe= 1,2-bis(diphenylphosphino)ethane), 2.56 Å for Cu metal)[10,20,21] but slightly shorter than the mean Cu−Cu distance in $[Cu_6Al_6](H)_4(Cp^*)_6$ (2.531 Å)[22] and very similar to the one in $[Cu_4Zn_4](CN^{t}Bu)_4(Cp^*)_3Cp$ (2.471 Å).[3] The longest M−M distances (avg. 2.75 Å) are observed between the central Cu4 atom and the Cu triangle spanned by Cu5, Cu6, and Cu7. The Cu−Zn distances (avg. 2.45 Å) are shorter with respect to $[Cu_4Zn_4](CN^{t}Bu)_4(Cp^*)_3Cp$ (2.498(2) Å)[3] but very similar to those in $[Cu_3Zn_4](Cp^*)_5$ (2.431(2)−2.458(2) Å),[5] reflecting the similar structural motifs of Zn capped Cu triangles. The Zn−$Cp^*_{centroid}$ distances are 1.91 and 1.92 Å, which are in line with literature values for terminal ZnCp* units in metal-rich molecules (1.83−2.19 Å) and especially comparable to those observed in $[Cu_3Zn_4](Cp^*)_5$ (1.901/1.922 Å).[5]

The six mesityl units are found in edge-bridging positions, each bridging one of the Cu−Cu contacts between the central Cu_3 triangle and the Cu_3 triangles of the two tetrahedral Cu_4 units. The Cu−C distances are all within the range of 1.992(5) and 2.044(4) Å and well in line with the Cu−C distance reported for $[Cu_5](Mes)_5$.[9]

Spectroscopic Characterization of ***2***. The ^{1}H- and ^{13}C NMR spectra of **2** in benzene-d^6 (see Figure S6) is consistent with the molecular structure found in the solid state and with all other analytical data. Due to the high sensitivity of **2**, small amounts of side products like mesitylene are found in the NMR spectra. The isotopic pattern of the molecular ion peak of **2** in the LIFDI mass spectrum is in agreement with the calculated isotopic pattern for $[Cu_{10}Zn_2](Mes)_6(Cp^*)_2$ (Figure 4).

Computational Analysis of ***2***. The assignment of the two zinc locations over 12 metal sites in **2** was obtained by geometry optimization based on total energy DFT calculations of 10 representative configurations (see Supporting Information, Figure S10) in the same manner as proceeded for **1** (see computational details and Figure S10). Following the same trend, there is an excellent structural agreement between the XRD structure and the lowest energy configuration, in which

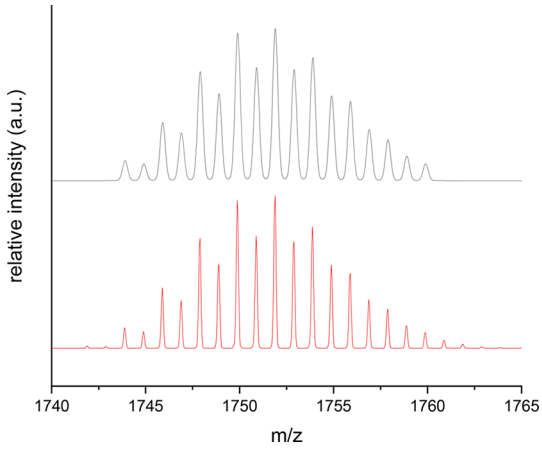

Figure 4. Comparison of the experimental (as determined by positive-ion-mode LIFDI-MS; bottom, red) and calculated (top, black) isotopic pattern of $[Cu_{10}Zn_2](Mes)_6(Cp^*)_2$ (**2**).

the two zinc atoms are located on the capping positions along the pseudo-threefold axis. In the same way as for **1**, this low energy configuration was then investigated at the BP86/TZ2P-D3 level with the ADF2017 code (see computational details, Supporting Information) for analyzing its electronic structure, which, as developed below, can be explained within the framework of the superatom concept.[23−25] The computed ^{1}H and ^{13}C NMR chemical shifts are also consistent with their experimental counterparts (Table S2). The first question that arises with respect to electron distribution is that of the metal oxidation states. Indeed, with six mesityl and two Cp* ligands, all formally anionic, the $[Cu_{10}Zn_2]$ group oxidation state is +8, that is, there are $[(10 \times 1) + (2 \times 2)] - 8 = 6$ metallic 4s electrons located somewhere on the metal core. This number is not a superatom closed-shell "magic" electron count, which makes sense owing to the fact that the regular superatom model assumes cluster spherical shapes,[23−25] which is obviously not the case for **2**. In any case, like in superatoms of group 11 metals, metal−metal bonding in **2** is expected to be mainly ensured by these valence s-type electrons.[24−26] Like in group 11 superatoms also, the computed HOMO−LUMO gap of **2** (1.51 eV), although significant, is not as large as that found usually at the GGA level for Cu(I) species.[27] A careful analysis of the occupied Kohn−Sham orbitals allowed identifying three of them with important 4s character, two of pseudo-a'_1 and one of pseudo-a''_2 symmetry. They are plotted in Figure 5. The highest one is the pseudo-a'_1 HOMO, which is principally composed of the 4s AO of the central Cu4 atom, with some minor antibonding admixture from the other metal atoms. The two other 4s combinations have significant bonding character and therefore much lower energies. The lowest is the pseudo-a'_1 bonding counterpart of the HOMO. The other one, of pseudo-a''_2 symmetry, is bonding within each of the inner Cu_4 tetrahedra. Thus, in terms of a superatomic description, the electron configuration of **2** is $1S^2\ 1P_z^2\ 2S^2$, consistent with the very prolate shape of the cluster core. Thus, despite its substantial deviation from spherical symmetry, we believe that the superatom model still appears to be a useful limit reference for rationalizing the electronic structure of **2**. Consistently, the two LUMOs can be tentatively identified as the $1P_{x,y}$ orbitals. The weakly antibonding 2s HOMO lies 0.76 eV above the HOMO−1, suggesting the possibility of oxidizing **2** without major structural change. The

https://dx.doi.org/10.1021/acs.inorgchem.0c00943
Inorg. Chem. XXXX, XXX, XXX−XXX

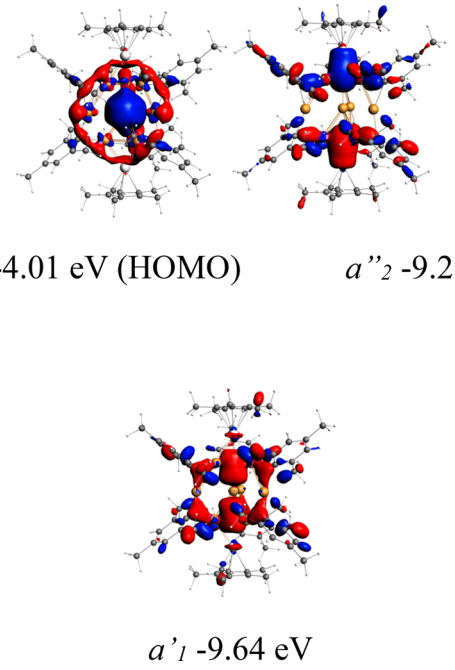

Figure 5. Three occupied orbitals of **2** of large 4s character responsible for metal−metal bonding in the $[Cu_{10}Zn_2]$ core.

Cu4 NAO charge (−0.47) is rather negative, indicative of an oxidation state close to −I, in agreement with the HOMO nature. That of the three outer Cu atoms (+0.63) is close to what is usually found for Cu(I).[27] The six other Cu atoms have an intermediate charge of +0.33. The Zn NAO charge (+0.97) is indicative of partly reduced Zn(II). Consistently, the Zn−Cu Wiberg indices are significant (avg. 0.197). The largest Cu−Cu Wiberg indices are within the two small triangles (avg. 0.151), and the smallest (avg. 0.043) correspond to the longest bonds, *i.e.*, between the central and most inner Cu atoms. Overall, **2** can be viewed as a very elongated superatom with an unusual electron count associated with this prolate distortion. This unexpected situation is likely to be associated with the bridging ability of the ZnCp* capping units that offer the possibility to strongly bind to the top and the bottom of the cluster in addition to the bridging mesityl ligands stabilizing the Cu core of the cluster.

CONCLUSIONS

Two new intermetallic Cu/Zn clusters with the cores M_{11} = $CuZn_{10}$ and M_{12} = $Cu_{10}Zn_2$ have been synthesized and characterized with either Cu or Zn as the dominating element in the cluster core, namely $[CuZn_{10}](Cp^*)_7$ = $[Cu(ZnZnCp^*)_3(ZnCp^*)_4]$ (**1**) and $[Cu_{10}Zn_2](Mes)_6(Cp^*)_2$ (**2**). The (mainly covalent) bonding situation in both clusters as investigated by detailed density functional theory analysis reveals interesting differences: The Zn-rich compound **1** can be regarded as an 18 valence-electron electron complex of Cu with emerging cluster bonding represented by its specific deviation from high symmetry (*e.g.*, pentagonal-bipyramidal). Similar closed-shell 18 VE systems with a more coordination compound bonding type, *e.g.*, $[MoZn_{12}](Me)_9(Cp^*)_3$ or $[PdZn_8](Cp^*)_4(Me)_4$, show ideal polyhedral (icosahedral or octahedral, respectively) symmetry, which underlines the unique character of **1** in our whole series or TM-centered all-organozinc-coordinated complexes. In accordance to this transition from a complex to a cluster, **1** exhibits fluxional behavior of the ZnZnCp* and ZnCp* groups. At room temperature, the ZnCp* units cannot be distinguished by NMR. In sharp contrast, compound **2**, which is obtained from the reaction of $[Cu_5](Mes)_5$ with $[Zn_2](Cp^*)_2$, exhibits a fully delocalized electronic structure typical for a cluster that can be described as a prolate distorted superatom with a $1S^2\ 1P_z^2\ 2S^2$ configuration. The new clusters **1** and **2** with a metal stoichiometry far away from typical Cu/Zn Hume−Rothery phases and a very low VEC (VEC(**1**) = (1 + 2 × 10 − 7)/11 = 1.27 and VEC(**2**) = (10 + 2 × 2) − 8/12 = 0.5) expand our series of Cu/Zn clusters (including of the general formula $\{[Cu_aZn_b](R)_c\}^k$, with M_n cores of n = 3, 7−12 (M = Cu, Zn; n = a + b, R = hydrocarbon ligand). All these clusters exhibit highly fascinating, unique molecular structures and bonding situations and contribute to our research concept of "intermetalloid clusters: molecules and solids in a dialogue".[28] Interestingly, evidence for small clusters with n = 4−6 is still missing, while some indications for the possible accessibility of larger clusters n > 12 can be deduced from *in situ* mass spectroscopic data of reaction mixtures. We thus expect many more species to be discovered following the strategy outlined in this and our previous reports.[3−5]

ASSOCIATED CONTENT

Supporting Information

The Supporting Information is available free of charge at https://pubs.acs.org/doi/10.1021/acs.inorgchem.0c00943.

Detailed description of materials and methods (including X-ray crystallography and computational details), crystallographic information for compounds **1** and **2**, computed NMR shifts for compound **2**, LIFDI-MS spectra, NMR spectra, Raman spectra, and optimized geometries for M_{11} and M_{12} (M = Cu, Zn) ligand protected clusters (PDF)

Accession Codes

CCDC 1993671−1993672 contain the supplementary crystallographic data for this paper. These data can be obtained free of charge via www.ccdc.cam.ac.uk/data_request/cif, or by emailing data_request@ccdc.cam.ac.uk, or by contacting The Cambridge Crystallographic Data Centre, 12 Union Road, Cambridge CB2 1EZ, UK; fax: +44 1223 336033.

AUTHOR INFORMATION

Corresponding Author

Roland A. Fischer − *Department of Chemistry and Catalysis Research Centre, Technical University Munich, D-85748 Garching, Germany;* orcid.org/0000-0002-7532-5286; Email: roland.fischer@tum.de

Authors

Max Schütz − *Department of Chemistry and Catalysis Research Centre, Technical University Munich, D-85748 Garching, Germany*

Maximilian Muhr − *Department of Chemistry and Catalysis Research Centre, Technical University Munich, D-85748 Garching, Germany;* orcid.org/0000-0002-6977-5002

Kerstin Freitag − *Department of Chemistry, Technical University Munich, D-85748 Garching, Germany*

Christian Gemel − *Department of Chemistry and Catalysis Research Centre, Technical University Munich, D-85748 Garching, Germany*

Samia Kahlal − *Univ Rennes, CNRS, F-35000 Rennes, France*

https://dx.doi.org/10.1021/acs.inorgchem.0c00943
Inorg. Chem. XXXX, XXX, XXX−XXX

Jean-Yves Saillard − *Univ Rennes, CNRS, F-35000 Rennes, France*
Augusto C. H. Da Silva − *São Carlos Institute of Chemistry, University of São Paulo, 13560-970 São Carlos, SP, Brazil*
Juarez L. F. Da Silva − *São Carlos Institute of Chemistry, University of São Paulo, 13560-970 São Carlos, SP, Brazil;* orcid.org/0000-0003-0645-8760
Thomas F. Fässler − *Department of Chemistry and Catalysis Research Centre, Technical University Munich, D-85748 Garching, Germany;* orcid.org/0000-0001-9460-8882

Complete contact information is available at: https://pubs.acs.org/10.1021/acs.inorgchem.0c00943

Author Contributions

The manuscript was written through contributions of all authors. All authors have given approval to the final version of the manuscript.

Funding

This work was supported by the Deutsche Forschungsgemeinschaft (grant Fi 502/23-2) as well as the TUM Global Incentive Fund.

Notes

The authors declare no competing financial interest.

■ ACKNOWLEDGMENTS

Kerstin Mayer, Carsten Aulenbacher, Christoph Wallach, and Christina Fischer are acknowledged for support in initial mass spectrometric measurements. Dr. Christian Jandl is acknowledged for help in the refinement of single crystal XRD data. S.K. and J.-Y.S. are grateful to GENCI (Grand Equipment National de Calcul Intensif) for HPC resources (Project A0050807367). A.C.H.S and J.L.F.S gratefully acknowledge support from FAPESP (São Paulo Research Foundation, Grant Numbers 2017/11631-2 and 2018/21401-7), Shell, and the strategic importance of the support given by ANP (Brazil's National Oil, Natural Gas and Biofuels Agency) through the R \&D levy regulation.

■ REFERENCES

(1) Gonzalez-Gallardo, S.; Bollermann, T.; Fischer, R. A.; Murugavel, R. Cyclopentadiene based low-valent group 13 metal compounds: Ligands in coordination chemistry and link between metal rich molecules and intermetallic materials. *Chem. Rev.* **2012**, *112* (6), 3136−3170.
(2) Gemel, C.; Steinke, T.; Cokoja, M.; Kempter, A.; Fischer, R. A. Transition metal chemistry of low valent group 13 organyls. *Eur. J. Inorg. Chem.* **2004**, *2004* (21), 4161−4176.
(3) Freitag, K.; Banh, H.; Gemel, C.; Seidel, R. W.; Kahlal, S.; Saillard, J.-Y.; Fischer, R. A. Molecular brass: Cu_4Zn_4, a ligand protected superatom cluster. *Chem. Commun.* **2014**, *50* (63), 8681−8684.
(4) Freitag, K.; Gemel, C.; Jerabek, P.; Oppel, I. M.; Seidel, R. W.; Frenking, G.; Banh, H.; Dilchert, K.; Fischer, R. A. The σ-Aromatic Clusters $[Zn_3]^+$ and $[Zn_2Cu]$: Embryonic Brass. *Angew. Chem., Int. Ed.* **2015**, *54* (14), 4370−4374.
(5) Banh, H.; Hornung, J.; Kratz, T.; Gemel, C.; Pöthig, A.; Gam, F.; Kahlal, S.; Saillard, J.-Y.; Fischer, R. A. Embryonic brass: pseudo two electron Cu/Zn clusters. *Chem. Sci.* **2018**, *9* (48), 8906−8913.
(6) Hollemann, A. F.; Wiberg, N. *Lehrbuch der Anorganischen Chemie*, 102nd ed.; de Gruyter, 2007; p 1408.
(7) Hume-Rothery, W.; Haworth, C. W.; Smallman, R. E. The Structure of Metals and Alloys. *The Structure of Metals and Alloys*, 5th ed.; The Institute of Metals: London, 1969.
(8) Grirrane, A.; Resa, I.; Rodriguez, A.; Carmona, E.; Alvarez, E.; Gutierrez-Puebla, E.; Monge, A.; Galindo, A.; del Río, D.; Andersen, R. A. Zinc- Zinc Bonded Zincocene Structures. Synthesis and Characterization of $Zn_2(\eta^5\text{-}C_5Me_5)_2$ and $Zn_2(\eta^5\text{-}C_5Me_4Et)_2$. *J. Am. Chem. Soc.* **2007**, *129* (3), 693−703.
(9) Meyer, E. M.; Gambarotta, S.; Floriani, C.; Chiesi-Villa, A.; Guastini, C. Polynuclear aryl derivatives of Group 11 metals. Synthesis, solid state-solution structural relationship, and reactivity with phosphines. *Organometallics* **1989**, *8* (4), 1067−1079.
(10) Jordan, A. J.; Wyss, C. M.; Bacsa, J.; Sadighi, J. P. Synthesis and reactivity of new copper (I) hydride dimers. *Organometallics* **2016**, *35* (5), 613−616.
(11) Cadenbach, T.; Bollermann, T.; Gemel, C.; Tombul, M.; Fernandez, I.; Hopffgarten, M. v.; Frenking, G.; Fischer, R. A. Molecular Alloys, Linking Organometallics with Intermetallic Hume-Rothery Phases: The Highly Coordinated Transition Metal Compounds $[M(ZnR)_n]$ ($n \geq 8$) Containing Organo- Zinc Ligands. *J. Am. Chem. Soc.* **2009**, *131* (44), 16063−16077.
(12) Bollermann, T.; Freitag, K.; Gemel, C.; Seidel, R. W.; von Hopffgarten, M.; Frenking, G.; Fischer, R. A. The Reactivity of $[Zn_2Cp^*_2]$: Trapping Monovalent {ZnZnCp*} in the Metal-Rich Compounds $[(Pd, Pt)(GaCp^*)_a(ZnCp^*)_{(4-a)}\ (ZnZnCp^*)_{(4-a)}]$(a= 0, 2). *Angew. Chem., Int. Ed.* **2011**, *50* (3), 772−776.
(13) Freitag, K.; Molon, M.; Jerabek, P.; Dilchert, K.; Rösler, C.; Seidel, R. W.; Gemel, C.; Frenking, G.; Fischer, R. A. Zn···Zn interactions at nickel and palladium centers. *Chem. Sci.* **2016**, *7* (10), 6413−6421.
(14) Blum, V.; Gehrke, R.; Hanke, F.; Havu, P.; Havu, V.; Ren, X.; Reuter, K.; Scheffler, M. Ab initio molecular simulations with numeric atom-centered orbitals. *Comput. Phys. Commun.* **2009**, *180* (11), 2175−2196.
(15) Perdew, J. P.; Burke, K.; Ernzerhof, M. Generalized gradient approximation made simple. *Phys. Rev. Lett.* **1996**, *77* (18), 3865.
(16) Te Velde, G. t.; Bickelhaupt, F. M.; Baerends, E. J.; Fonseca Guerra, C.; van Gisbergen, S. J.; Snijders, J. G.; Ziegler, T. Chemistry with ADF. *J. Comput. Chem.* **2001**, *22* (9), 931−967.
(17) Baerends, E. ADF2016, SCM. 2016. *Theoretical Chemistry*; Vrije Universiteit: Amsterdam, The Netherlands.
(18) Berry, R.; Raynor, G. V. The crystal chemistry of the Laves phases. *Acta Crystallogr.* **1953**, *6* (2), 178−186.
(19) Steinke, T.; Gemel, C.; Winter, M.; Fischer, R. A. The Clusters $[M_a(ECp^*)_b]$(M= Pd, Pt; E= Al, Ga, In): Structures, Fluxionality, and Ligand Exchange Reactions. *Chem. - Eur. J.* **2005**, *11* (5), 1636−1646.
(20) Wei, Q.-H.; Yin, G.-Q.; Zhang, L.-Y.; Shi, L.-X.; Mao, Z.-W.; Chen, Z.-N. Luminescent Ag^I- Cu^I Heterometallic Hexa-, Octa-, and Hexadecanuclear Alkynyl Complexes. *Inorg. Chem.* **2004**, *43* (11), 3484−3491.
(21) Beck, J.; Strähle, J. Complexes of 1,5-Di(p-tolyl)-1,4-pentaazadien-3-ide, Crystal Structures of $[Cu(tolylNNNNNtolyl)]_3$ and $[Ni(tolylNNNNNtolyl)_2]_2$. *Angew. Chem., Int. Ed. Engl.* **1985**, *24* (5), 409−410.
(22) Ganesamoorthy, C.; Weßing, J.; Kroll, C.; Seidel, R. W.; Gemel, C.; Fischer, R. A. The Intermetalloid Cluster $[(Cp^*AlCu)_6H_4]$, Embedding a Cu_6 Core Inside an Octahedral Al_6 Shell: Molecular Models of Hume-Rothery Nanophases. *Angew. Chem., Int. Ed.* **2014**, *53* (30), 7943−7947.
(23) Khanna, S.; Jena, P. Atomic clusters: Building blocks for a class of solids. *Phys. Rev. B: Condens. Matter Mater. Phys.* **1995**, *51* (19), 13705.
(24) Walter, M.; Akola, J.; Lopez-Acevedo, O.; Jadzinsky, P. D.; Calero, G.; Ackerson, C. J.; Whetten, R. L.; Grönbeck, H.; Häkkinen, H. A unified view of ligand-protected gold clusters as superatom complexes. *Proc. Natl. Acad. Sci. U. S. A.* **2008**, *105* (27), 9157−9162.
(25) Häkkinen, H. Atomic and electronic structure of gold clusters: understanding flakes, cages and superatoms from simple concepts. *Chem. Soc. Rev.* **2008**, *37* (9), 1847−1859.
(26) Sharma, S.; Chakrahari, K. K.; Saillard, J.-Y.; Liu, C. Structurally Precise Dichalcogenolate-Protected Copper and Silver Superatomic

Nanoclusters and Their Alloys. *Acc. Chem. Res.* **2018**, *51* (10), 2475−2483.
(27) Dhayal, R. S.; Liao, J. H.; Wang, X.; Liu, Y. C.; Chiang, M. H.; Kahlal, S.; Saillard, J. Y.; Liu, C. Diselenophosphate-Induced Conversion of an Achiral $[Cu_{20}H_{11}\{S_2P(OiPr)_2\}_9]$ into a Chiral $[Cu_{20}H_{11}\{Se_2P(OiPr)_2\}_9]$ Polyhydrido Nanocluster. *Angew. Chem., Int. Ed.* **2015**, *54* (46), 13604−13608.
(28) Mayer, K.; Weßing, J.; Fässler, T. F.; Fischer, R. A. Intermetalloid Clusters: Molecules and Solids in a Dialogue. *Angew. Chem., Int. Ed.* **2018**, *57*, 14372−14393.

https://dx.doi.org/10.1021/acs.inorgchem.0c00943
Inorg. Chem. XXXX, XXX, XXX−XXX